Identifying hydrocarbons with FWI-derived angle gathers from an augmented wave equation

K. Torres[1], J. McLeman[1]

[1] DUG Technology

Summary

A full-waveform inversion (FWI) framework that embeds angle-dependent scattering effects directly into the wave equation as explicit, invertible parameters through an augmented acoustic formulation is presented. In contrast to conventional workflows that rely on pre-imaging angle decomposition or offset-based data partitioning, the proposed method generates subsurface angle gathers natively within the inversion by computing stabilised reflection angles locally in space and time from the propagating wavefield.

The approach is validated using both a synthetic experiment and a 3D field dataset, demonstrating its ability to recover physically consistent amplitude-versus-angle (AVA) behaviour directly from the raw field data. The inverted gathers exhibit coherent amplitude variation with angle across hydrocarbon-bearing intervals, while derived AVA attributes show laterally continuous and geologically consistent responses that align with known reservoir features and lithologic variations. These results show that using the augmented acoustic wave equation provides a robust, interpretable, and kinematically meaningful representation of angle-dependent imaging products, offering a unified least-squares framework for AVA analysis within FWI.

Identifying hydrocarbons with FWI-derived angle gathers from an augmented wave equation

Introduction

Full-waveform inversion (FWI) has revolutionised seismic imaging by enabling the recovery of high-resolution subsurface models through the iterative minimisation of the misfit between wave-equation-simulated and field data. Beyond velocity model building, FWI-based imaging has demonstrated the ability to produce reflectivity images with improved spatial resolution compared to conventional migration workflows. Recent studies have further shown that acoustic FWI-derived imaging products can preserve amplitude trends consistent with elastic theory, while often yielding cleaner and better-illuminated angle stacks due to the direct use of the raw field data (e.g., McLeman et al., 2021; Warner et al., 2022). In many of these approaches, angle information is typically introduced through approximate offset- or angle-based data-domain partitioning prior to inversion, or through modified objective functions designed to emphasise selected angle ranges in the data-domain.

In this work, we present an alternative formulation that recovers angle-dependent model updates within the FWI framework. By augmenting the acoustic wave equation, subsurface angle gathers are generated directly during the inversion, avoiding the computational expense of performing separate wavefield simulations for each angle range. Unlike pre-imaging angle mutes, which are defined based on the incidence angle of primary reflections and are therefore not strictly valid for multiples, the proposed approach computes stabilised reflection angles locally in space and time during wavefield propagation and assigns energy to user-defined angle bins. As a result, angle-dependent imaging products are constructed from the full wavefield, considering primaries, multiples, and ghosts, within a single least-squares inversion.

Theory

The proposed approach uses the generalised expansion of the acoustic wave equation (McLeman et al., 2021), expressed in the isotropic case as

$$\frac{1}{v_p(\mathbf{x})^2}\frac{\partial^2 u(\mathbf{x},t)}{\partial t^2} - \nabla^2 u(\mathbf{x},t) + \sum_{j=1}^{N} \nabla r_j(\mathbf{x}) \cdot \left(d_j(\mathbf{x},t)\nabla u(\mathbf{x},t)\right) = s(t)\delta(\mathbf{x}-\mathbf{x}_0), \tag{1}$$

where v_p is the P-wave velocity, u is the pressure wavefield, s represents the scaled source term, $\mathbf{x}_0$ indicates the source position, and r_j and d_j denote scattering parameters and associated directivity terms, respectively. The integer N controls the number of directional scattering terms retained in the augmented wave equation and the number of secondary source terms. In the standard variable-density formulation, the last term on the left-hand side of equation (1) reduces to $\nabla \log \rho \cdot \nabla u$, which accounts for scattering induced by spatial variations in $\log \rho$.

To make the angular dependence of scattering explicit and invertible at the wave-equation level, we parameterise the scattering terms using angle-dependent proxy components, $r_j(\mathbf{x}) = \log \rho_j(\mathbf{x})$, and define the directivities as angle-dependent weights, $d_j(\mathbf{x},t) = w_j(\theta(\mathbf{x},t))$. The index j labels predefined angle bins, and $w_j(\theta)$ represents bin indicator functions or tapering weights localised to the j-th reflection angle range, with θ denoting a kinematically derived reflection angle. With this choice, the resulting wave equation is given by

$$\frac{1}{v_p(\mathbf{x})^2}\frac{\partial^2 u(\mathbf{x},t)}{\partial t^2} - \nabla^2 u(\mathbf{x},t) + \sum_{j=1}^{N} w_j(\theta(\mathbf{x},t))\nabla \log \rho_j(\mathbf{x}) \cdot \nabla u(\mathbf{x},t) = s(t)\delta(\mathbf{x}-\mathbf{x}_0), \tag{2}$$

which can also be extended to anisotropic symmetries.

The inverse problem relating the scattering proxies $\mathbf{m} = [\log \rho_1, \ldots, \log \rho_N]$ to the field data $\mathbf{d}$ can be expressed as the minimisation of the objective function $E(\mathbf{m})$

$$E(\mathbf{m}) = \frac{1}{2}||\mathbf{d} - \mathbf{L}(\mathbf{m})||^2, \tag{3}$$

where $\mathbf{L}(\cdot)$ is the nonlinear forward modelling operator defined by equation (2) and $||\cdot||$ denotes the ℓ_2-norm. Gradients with respect to $\log \rho_j$ are computed using the adjoint-state method.

In this formulation, angle gathers emerge naturally from the inversion variables, which encode the scattering information needed to match the angular dependence present in the field data. Reflectivity attributes are then derived as functions of the velocity model and the inverted angle-dependent scattering parameters. In the results shown, the velocity is assumed to be fixed; however, the formulation does not prevent simultaneous inversion with velocity (and other subsurface parameters). Image-domain constraints based on angle-gather move-out can also be used to refine the velocity model further. The reflection angle is computed as

$$\theta(\mathbf{x}, t) = \arccos\left(\mathbf{P}(\mathbf{x}, t) \cdot \mathbf{n}(\mathbf{x})\right), \tag{4}$$

where $\mathbf{P}$ denotes the normalised Poynting vector, and $\mathbf{n}$ is the local reflector normal obtained, for example, from precomputed dip fields, migrated sections, or from the updated models. To mitigate instabilities arising from wavefield zero-crossings, the Poynting vectors may be stabilised using additional regularisation strategies. Figure 1 shows the seismic response (forward wavefield simulation and shot gather) for a single flat reflecting interface with a prescribed angular variation in reflection polarity at approximately 25°. This illustration demonstrates that the augmented wave equation can encode an arbitrary angular variability in the scattering response within an acoustic setting.

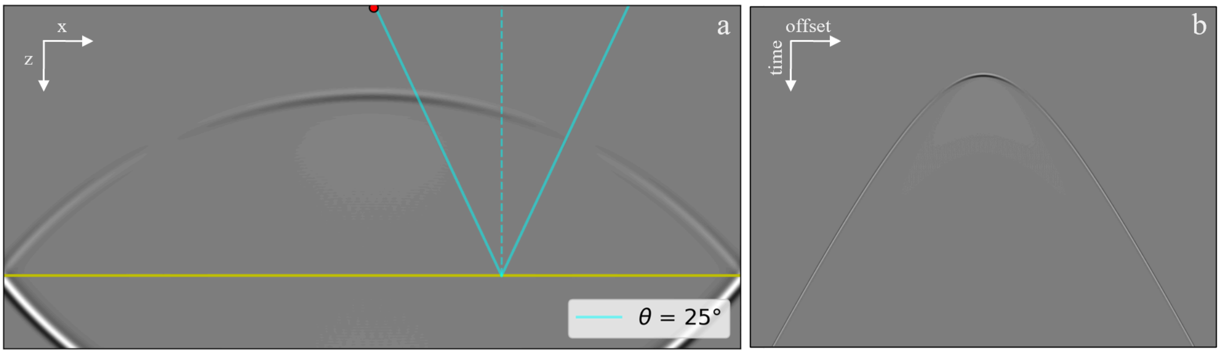

Figure 1 *(a) Wavefield snapshot and (b) synthetic surface seismogram for a single reflecting interface (yellow line) exhibiting an AVA polarity reversal. The red dot indicates the source position.*

Examples

The approach is first validated using a controlled synthetic experiment designed to test AVA consistency. Acoustic and elastic datasets are generated in a constant-velocity medium with a four-layer density model, such that reflections are driven exclusively by density contrasts. For the acoustic dataset, the standard variable-density acoustic wave equation is employed for input generation. For the elastic dataset, a fixed value of $v_s/v_p = 0.5$ is used. Both datasets are inverted using 10 angle bins spanning the range [0°, 50°], starting from a constant-density initial model.

Figure 2 shows the inverted gathers obtained after a few iterations of the proposed method for acoustic and elastic inputs. With the correct velocity, the acoustic-input inversion exhibits an approximately flat angle-independent response (as expected). In contrast, the elastic-input inversion displays a cosine-squared amplitude decay with angle, as predicted by linearised elastic theory for a density-only contrast. Scaling the acoustic result by $\cos^2(\theta)$ yields an AVA trend consistent with the elastic inversion. This experiment confirms that the proposed formulation recovers the elastic AVA.

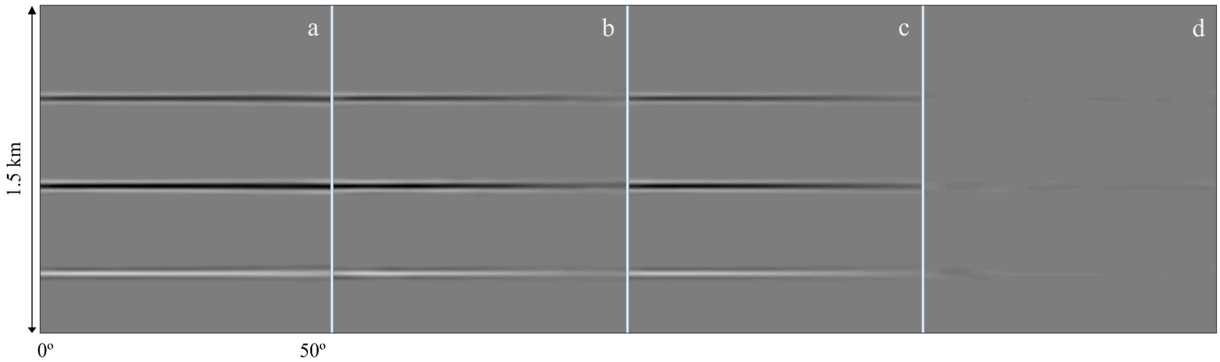

Figure 2 *Inverted angle gathers for the synthetic experiment: (a) acoustic input, (b) elastic input, (c) scaled acoustic result, and (d) difference between scaled acoustic and elastic results.*

The second example involves a 3D towed-streamer field dataset from the Australian North West Shelf with a maximum offset of 6 km. The proposed workflow is applied using frequencies up to 30 Hz, with the background velocity and initial density models taken from a prior multi-parameter FWI run with frequency continuation from 7 Hz to 12 Hz. The analysis is restricted to the angle range [0°, 45°], discretised into nine bins with Δθ=5°. The input is the raw field data, containing primaries, ghosts and multiples.

Figure 3 shows a stacked inline section derived from the angle-dependent FWI results, revealing the shallow carbonate heterogeneities and complex channel features that characterise the survey area. Figure 4 presents representative inverted angle gathers along the full section, spaced every 500 meters. Within the gas-bearing interval (yellow circles in Figures 3 and 4), the gathers exhibit coherent reflection events with stable amplitudes across the sampled angle range. Furthermore, residual moveout curvature observed in some reflection events (red arrows in Figure 4) indicates sensitivity to background kinematics arising from velocity inaccuracies. Thus, the recovered gathers can provide a practical diagnostic for assessing and guiding velocity (and anisotropy) model updates.

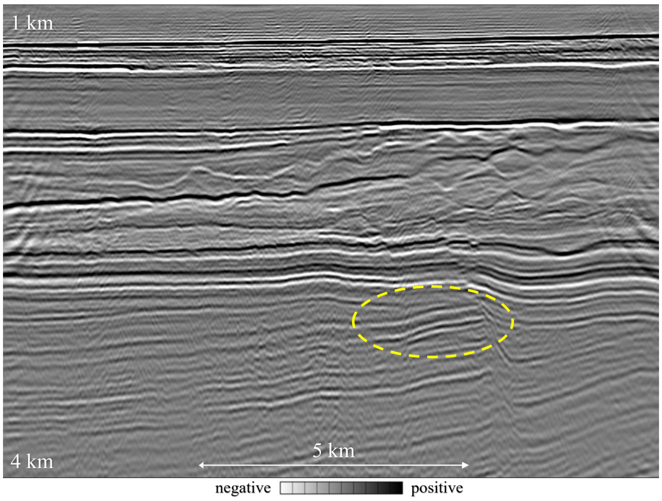

Figure 3 *Stack of angle gathers derived from the angle-dependent FWI results for the field dataset.*

AVA attributes computed from near, mid and far angle stacks are shown in Figure 5. The intercept and gradient volumes exhibit spatially continuous responses, and their cross-product readily identifies a localised anomaly coincident with the known gas-bearing region (black arrow).

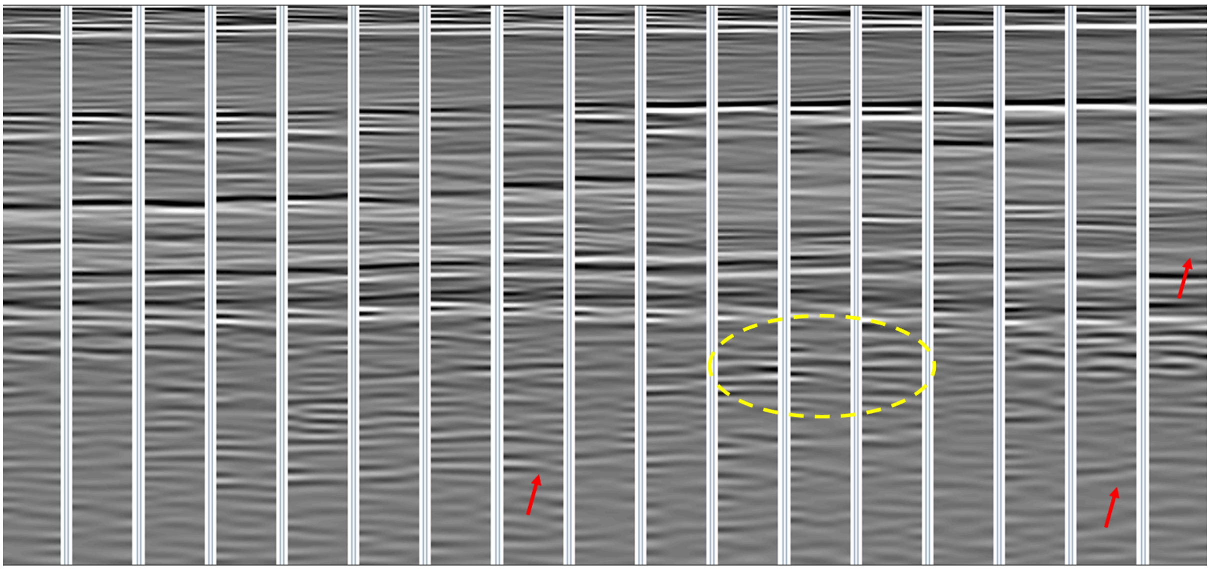

Figure 4 *Inverted angle gathers along the inline section, showing systematic amplitude variation with angle at the gas-bearing interval (yellow circle).*

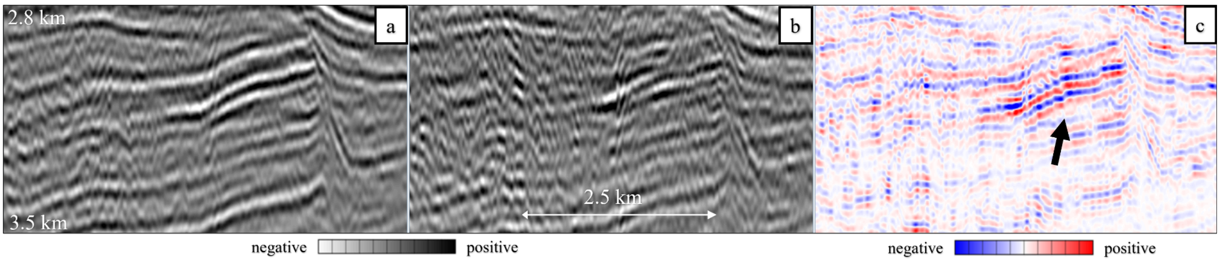

Figure 5 *(a) AVA Intercept, (b) gradient, and (c) intercept-gradient cross-product derived from the field dataset inversion results.*

Conclusions

By using the augmented acoustic wave equation, we introduced an inversion framework that explicitly incorporates angle dependence within FWI. The method directly recovers angle-dependent subsurface models without requiring prior angle decomposition in the data domain. The AVA attributes and angle gathers provide mutually consistent evidence that the proposed workflow recovers stable and interpretable AVA directly from raw field data. This method can also be readily extended to elastic wave-equation propagators and can serve as a QC for the correctness of inverted parameters.

Acknowledgements

We thank DUG Multi-Client for permission to use the BEX MC3D real data example and DUG Technology for permission to present this work.

References

McLeman, J., Burgess, T., Sinha, M., Hampson, G., & Thompson, T. [2021]. Reflection FWI with an augmented wave equation and quasi-Newton adaptive gradient scheme. First International Meeting for Applied Geoscience & Energy, 667-671

Warner, M., Armitage, J., Umpleby, A., Shah, N., Debens, H. and Mancini, F. [2022]. AVO determination using acoustic FWI. 83rd EAGE Conference & Exhibition, Extended Abstracts.